Spatiotemporal Analysis of Flow-Induced Intermediate Filament Displacement in Living Endothelial Cells

Brian P. Helmke,*† David B. Thakker,*† Robert D. Goldman,‡ and Peter F. Davies*†§
*Institute for Medicine and Engineering, †Department of Bioengineering, and §Department of Pathology and Laboratory Medicine, University of Pennsylvania, Philadelphia, Pennsylvania 19104; and ‡Department of Cell and Molecular Biology, Northwestern University Medical School, Chicago, Illinois 60611 USA

ABSTRACT The distribution of hemodynamic shear stress throughout the arterial tree is transduced by the endothelium into local cellular responses that regulate vasoactivity, vessel wall remodeling, and atherogenesis. Although the exact mechanisms of mechanotransduction remain unknown, the endothelial cytoskeleton has been implicated in transmitting extracellular force to cytoplasmic sites of signal generation via connections to the lumenal, intercellular, and basal surfaces. Direct observation of intermediate filament (IF) displacement in cells expressing green fluorescent protein-vimentin has suggested that cytoskeletal mechanics are rapidly altered by the onset of fluid shear stress. Here, restored images from time-lapse optical sectioning fluorescence microscopy were analyzed as a four-dimensional intensity distribution function that represented IF positions. A displacement index, related to the product moment correlation coefficient as a function of time and subcellular spatial location, demonstrated patterns of IF displacement within endothelial cells in a confluent monolayer. Flow onset induced a significant increase in IF displacement above the nucleus compared with that measured near the coverslip surface, and displacement downstream from the nucleus was larger than in upstream areas. Furthermore, coordinated displacement of IF near the edges of adjacent cells suggested the existence of mechanical continuity between cells. Thus, quantitative analysis of the spatiotemporal patterns of flow-induced IF displacement suggests redistribution of intracellular force in response to alterations in hemodynamic shear stress acting at the lumenal surface.

INTRODUCTION

Endothelial cells (ECs) lining the artery wall respond to changes in hemodynamic shear stress acutely by mediation of vasoregulatory events in the underlying vessel wall and chronically by adaptation of morphology and gene and protein expression (Davies, 1995; Resnick et al., 1997; Chien et al., 1998). Although the mechanisms by which ECs sense changes in the mechanical environment remain unknown, several recent studies have proposed that the cytoskeleton and associated linking complexes serve as principal pathways for force transmission throughout the cytoplasm (Ingber, 1991; Davies, 1995). Applied extracellular force can be transmitted via integrin linkages (Burridge and Chrzanowska-Wodnicka, 1996; Schmidt et al., 1998) and redistributed both globally and locally (Ingber, 1991; Choquet et al., 1997; Heidemann et al., 1999). Thus, it is likely that cytoskeletal deformation or adaptation in response to spatial variation in hemodynamic shear stress represents an intracellular force redistribution that plays a role in the integration of mechanotransduction pathways.

Recent in vitro models have demonstrated cytoskeletal adaptation in ECs fixed after exposure to shear stress for discrete time periods (Dewey et al., 1981; Levesque and Nerem, 1985; Malek and Izumo, 1996; Galbraith et al., 1998). On a time scale of hours, alignment of cytoskeletal filaments and elongation of cell shape parallel to the flow direction have been measured. However, redistribution of forces within the cell may occur within seconds to minutes after extracellular force application. Cytoskeleton movement in living cells can be observed through the use of green fluorescent protein (GFP) (Doyle and Botstein, 1996; Carminati and Stearns, 1997; Westphal et al., 1997; Ballestrem et al., 1998; Ho et al., 1998; Yoon et al., 1998). Our recent observations of intermediate filament (IF) displacement in ECs during onset of shear stress suggest that extracellular forces acting on the lumenal membrane are redistributed within minutes to other intracellular sites (Helmke et al., 2000).

Because IFs are displaced heterogeneously at various locations within the cytoplasm (Helmke et al., 2000), a quantitative method to evaluate the spatial and temporal distribution of cytoskeletal movement is needed. Previous methods have emphasized measurement of orientation (Nerem et al., 1981; Petroll et al., 1993; Palmer and Bizios, 1997; Karlon et al., 1999) and/or shape (Nerem et al., 1981) at a cellular length scale using manual methods (Nerem et al., 1981; Galbraith et al., 1998), Fourier analysis (Palmer and Bizios, 1997), or intensity gradients in real space (Karlon et al., 1999). Significant changes in whole-cell parameters were measured only at a longer time scale (hours). However, measurements at a subcellular length scale are necessary to describe local displacement of cytoskeletal filament networks that may be relevant to intracellular force transmission or transduction. Here an automated image-processing method is introduced that computes the three-

---

Received for publication 17 July 2000 and in final form 3 October 2000.

Address reprint requests to Dr. Peter F. Davies, Institute for Medicine and Engineering, University of Pennsylvania, 1010 Vagelos Research Labs, 3340 Smith Walk, Philadelphia, PA 19104-6383. Tel.: 215-898-4647; Fax: 215-573-6815; E-mail: pfd@pobox.upenn.edu.

0006-3495/01/01/184/11 $2.00

dimensional (3-D) product moment cross-correlation (PMCC) as a function of subcellular spatial location and time. An algorithm implemented in Matlab software computes PMCC as a quantitative measure of fluorescence intensity spatial covariance among 3-D image pairs. A displacement index (DI) is defined that objectively describes regional IF movement independently of fluorescence intensity magnitude. Spatial and temporal variations in DI reveal patterns of endothelial cytoskeleton movement in response to onset of shear stress.

MATERIALS AND METHODS

Cell culture and transfection

A plasmid encoding GFP fused to the N-terminus of human vimentin (pEGFP-hVIM-Myc) (Yoon et al., 1998) was transfected into bovine aortic ECs using a liposomal method (Lipofectin, Gibco, Gaithersburg, MD) according to the manufacturer's recommendations. Briefly, ECs plated at 1×10^{-4} to 2×10^{-4} cells cm^{-2} were treated for 2.5 h with low-serum medium (Opti-MEM I, Gibco) containing 1–2 μg of plasmid and 14 μg of Lipofectin. Cells were allowed to recover overnight in complete growth medium (Dulbecco's modified Eagle's medium supplemented with 10% heat-inactivated calf serum). In some experiments, a cell line with stable expression of GFP-vimentin was established by treatment with 400 μg ml^{-1} G418 (Gibco) beginning 2 days after transfection. Because the plasmid contained a kanamycin/neomycin resistance gene (Yoon et al., 1998), only cells expressing GFP-vimentin survived the selection pressure. Groups of cells expressing similar levels of fluorescence intensity were isolated and grown to confluence.

Glass coverslips (Bioptechs, Butler, PA) were washed in Sparkleen detergent solution, rinsed with deionized water, and autoclaved. A suspension of 0.1-μm-diameter red fluorescent microspheres (Molecular Probes, Eugene, OR) was dried onto the coverslips so that microspheres adhered to the glass and served as fiducial markers for coverslip position during image acquisition (Fig. 1, *arrows*). Cells expressing GFP-vimentin were plated onto the coverslips over the microspheres and allowed to grow to confluence. All experiments were performed with confluent monolayers of cells.

Flow loop and flow chamber assembly

Coverslips with ECs expressing GFP-vimentin were assembled into a heated parallel plate flow chamber (Bioptechs) and were maintained at 37°C. The chamber had rectangular geometry with height (h) 0.25 mm, width (w) 14 mm, and length (l) 22 mm. A T-shaped header region served to spread flow entering the chamber, thereby minimizing entrance effects. Thus, flow through the chamber was fully developed steady Poiseuille flow. The wall shear stress imposed on the cells was computed as $\tau_w = 6\,\mu Q/wh^2$, where μ is fluid viscosity and Q is volume flow rate (Batchelor, 1967). In the present studies, Q was adjusted so that $\tau_w = 12$ dyn cm^{-2}, which corresponds to physiological arterial values. The Reynolds number with respect to chamber height was computed from $Re = \rho\tau_w h^2/6\,\mu^2$, where ρ is fluid density (Batchelor, 1967). In these studies, $Re < 10$ so that viscous drag forces dominated inertial forces and assumptions for Poiseuille flow were valid.

The flow chamber was assembled into a closed loop that consisted of an upstream reservoir, the flow chamber mounted on a microscope stage, a downstream reservoir, and a peristaltic pump that recirculated medium to the upstream reservoir. Fluid flow was driven by gravity from the upstream reservoir, which was placed at a height above the flow chamber calibrated to generate the desired flow rate. The downstream reservoir was placed in a water bath maintained at 37°C, and a humidified 5% CO_2/95% air mixture was equilibrated with the fluid surface to maintain pH.

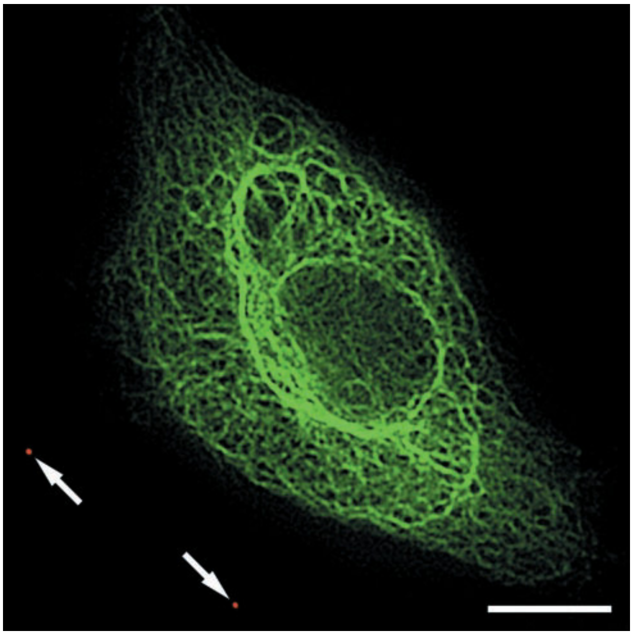

FIGURE 1 Distribution of GFP-vimentin (*green*) in an EC within a confluent monolayer. Neighboring cells not expressing GFP-vimentin are not visible. Volume projection of 3-D fluorescence optical sections after image restoration. Red fluorescent microspheres (*arrows*) were used in time-lapse studies to subtract coverslip movement. Scale bar, 10 μm.

Image acquisition

Wide-field fluorescence optical sections were acquired using a DeltaVision system (Applied Precision, Issaquah, WA) that consisted of a mercury arc illumination source, a Zeiss 63X/1.4NA Plan Apochromat objective lens, a cooled CCD camera (Princeton Instruments, Trenton, NJ), and appropriate barrier filter sets (Chroma, Brattleboro, VT) for GFP (λ_{ex} = 490 nm; λ_{em} = 528 nm) and red fluorescent microspheres (λ_{ex} = 555 nm; λ_{em} = 617 nm). Spatial and temporal normalization of the illumination intensity allowed quantitative analysis of GFP-vimentin fluorescence intensity (Hiraoka et al., 1990; Kam et al., 1993).

After flow loop assembly and chamber placement on the microscope stage, cells were selected that expressed GFP-vimentin distributed to the endogenous IF network. Dual-wavelength 3-D image stacks with 0.25–0.50-μm spacing between optical sections were acquired every 3 min for 20–30 min. A step change in flow was imposed so that $\tau_w = 12$ dyn cm^{-2}, and image acquisition continued at the same rate for an additional 20–30 min.

Image processing

A quantitative method for image restoration improved the spatial precision of IF locations over that typically measured by wide-field fluorescence microscopy. A point spread function, which describes the 3-D distribution of light emitted from a diffraction-limited point source of fluorescence, was measured experimentally. A constrained iterative deconvolution algorithm (Hiraoka et al., 1990) was applied to 3-D arrays of optical sections to reposition out of focus light. This image restoration method yielded a high-resolution spatial distribution of fluorescence intensity. Image restoration and volume projections were computed using SoftWoRx software (Applied Precision).

A coplanar set of red fluorescent microspheres on the coverslip was chosen as a fiducial reference, and the 3-D positions within each image stack were determined. Three-dimensional image volumes containing GFP-vimentin fluorescence were chosen so that positions along the x, y, and z axes were normalized relative to those of the microspheres. In this manner, movement of GFP-vimentin fluorescence in the time-lapse analysis was attributable only to IF displacement and not to coverslip movement. Four-dimensional analysis was performed on images containing one to four cells from each of six experiments.

Mathematical processing

Deconvolved, position-normalized image sets were exported from SoftWoRx software as 8-bit multi-page TIFF files for mathematical analysis using Matlab (MathWorks, Natick, MA). For each point (x, y, z) in 3-D image space, the fluorescence intensity distribution as a function of time was represented as $f(x, y, z, t)$. Thus, the 4-D distribution function f represents the IF network position in space and time.

To establish an appropriate length scale for subcellular analysis of IF segment movement, the power spectrum of a 3-D image set at the beginning of an experiment was analyzed. The 3-D discrete Fourier transform of an image set with dimensions $n_x \times n_y \times n_z$ was computed as

$$F(u, v, w) = \sum_{x=0}^{n_x-1} \sum_{y=0}^{n_y-1} \sum_{z=0}^{n_z-1} f(x, y, z) \exp\left[-2\pi i\left(\frac{ux}{n_x} + \frac{vy}{n_y} + \frac{wz}{n_z}\right)\right], \quad (1)$$

where (u, v, w) corresponds to the frequency domain coordinate position for (x, y, z) and $i = (-1)^{1/2}$. The power spectrum magnitude is given by $S = FF^*$, where F^* is the complex conjugate of F. The spectral density S was transformed to cylindrical coordinates, $S(r, \theta, w)$, where $r^2 = u^2 + v^2$ and $\tan\theta = v/u$. To determine the frequency response along the r axis, $S(r)$ was computed as the integral of $S(r, \theta, w)$ over all θ and w values. A local maximum was measured that corresponded to an average separation between IF segments in real space of 16 pixels (~1.7 μm). The integral of S over the $r\theta$ plane, $S(w)$, produced a local maximum corresponding to the resolution along the optical axis (~0.68 μm). For the subsequent regional analysis, subimages were chosen that had twice these dimensions (32 × 32 × 16 pixels) to prevent aliasing (see Fig. 3).

The degree of overlap between spatial distributions of fluorescence at two time points indicates the degree of displacement of the GFP-vimentin-labeled IFs contained in the spatial region. It is convenient to measure the degree of overlap between images at times t_i and t_j using the cross-product moment (spatial covariance):

$$\mathrm{Cov}[f(x, y, z, t_i), f(x, y, z, t_j)] = \frac{1}{n_x n_y n_z} \sum_{x=1}^{n_x} \sum_{y=1}^{n_y} \sum_{z=1}^{n_z} \left[\left(f(x, y, z, t_i) - \overline{f(x, y, z, t_i)}\right)\left(f(x, y, z, t_j) - \overline{f(x, y, z, t_j)}\right)\right], \quad (2)$$

where

$$\overline{f(x, y, z, t)} = \frac{1}{n_x n_y n_z} \sum_{x=1}^{n_x} \sum_{y=1}^{n_y} \sum_{z=1}^{n_z} f(x, y, z, t)$$

is the mean intensity in the 3-D image at time t. To eliminate the dependence of the covariance on the number of non-zero data points and the absolute intensity scale, it is normalized by the product of the variances, where the variance at time t is given by

$$\mathrm{Var}[f(x, y, z, t)] = \frac{1}{n_x n_y n_z} \sum_{x=1}^{n_x} \sum_{y=1}^{n_y} \sum_{z=1}^{n_z} \left(f(x, y, z, t) - \overline{f(x, y, z, t)}\right)^2. \quad (3)$$

The product moment correlation coefficient is defined using Eqs. 2 and 3 as

$$\mathrm{PMCC}(t_i, t_j) = \frac{\mathrm{Cov}[f(x, y, z, t_i), f(x, y, z, t_j)]}{\left(\mathrm{Var}[f(x, y, z, t_i)]\ \mathrm{Var}[f(x, y, z, t_j)]\right)^{1/2}}. \quad (4)$$

Eq. 4 gives a normalized measure of degree of overlap of the 3-D IF network structure at times t_i and t_j. Note that this is invariant with respect to the absolute intensity scale and the number of non-zero data points.

Finally, a displacement index (DI) was computed from

$$\mathrm{DI}(t_i, t_j) = 1 - \mathrm{PMCC}(t_i, t_j). \quad (5)$$

For pairs of 3-D fluorescence intensity distribution functions measured at distinct time points, values for the DI lie in the interval [0,1]. A value of zero corresponds to high spatial overlap in IF positions, or zero displacement; a value of one indicates that IF positions at the end of a time interval are not correlated to the initial positions.

Computation of PMCC was implemented in Matlab script language, enabling automation of results and output. PMCC data were imported into Excel workbooks for DI computations and statistical analysis, as described below.

Statistical analysis

To perform statistical analysis, the Fisher approximation for the probability distribution function of the PMCC was used (davidmlane.com/hyperstat). PMCC values were transformed using the equation

$$z' = 0.5 \times \ln\left(\frac{1 + \mathrm{PMCC}}{1 - \mathrm{PMCC}}\right). \quad (6)$$

The transformed variable z' is approximately normally distributed. The mean and 95% confidence limits for z' were computed and transformed back into expected values and confidence intervals using the inverse Fisher transformation:

$$\mathrm{PMCC} = \frac{e^{2z'} - 1}{e^{2z'} + 1}. \quad (7)$$

All-pairwise comparisons among spatially grouped z' values were performed using the Newman-Keuls procedure. Results are reported as significant differences in expected values of DI when $p < 0.05$.

RESULTS

Flow-induced regional deformation of IFs

GFP-vimentin transiently expressed in bovine aortic ECs was incorporated into the endogenous vimentin IF network (Blose and Meltzer, 1981; Helmke et al., 2000). As illustrated in a volume projection image (Fig. 1), IF bundles of varying thickness and length formed a complex interconnected mesh throughout the cytoplasm, and thicker bundles were frequently observed in the perinuclear region. Cells expressing GFP-vimentin were frequently surrounded by neighboring cells in the confluent monolayer that were not expressing the fluorescent protein. This allowed analysis of movement within single cells in the monolayer. During time-lapse experiments, 0.1-μm red fluorescent microspheres (Fig. 1, *arrows*) served as fiducial markers of coverslip position to correct for systematic movement in the IF motion analysis.

Constitutive motion of GFP-vimentin in ECs was observed even in the absence of flow (Helmke et al., 2000), indicating that IFs form a dynamic cytoskeletal network. However, the onset of unidirectional laminar shear stress across the endothelial surface induced significant deformation of regions of IF segments (Fig. 2) that was superimposed on constitutive motion. In merged color images, IF positions were compared just before (Fig. 2, red) and 3 min after (Fig. 2, green) flow onset; yellow represented zero displacement during the interval. Near the coverslip (Fig. 2, *A–C*), heterogeneous displacement of IFs was measured. Movement of adjacent filament segments consisted of translation and bending or flexing (Fig. 2 *B*) . In some regions, groups of filaments underwent coordinated translation with a minimum of mesh deformation (Fig. 2 *C*). Interestingly, filaments in this region moved with direction and magnitude similar to those in the neighboring cell (Fig. 2 *B*, right side), suggesting that a mechanical link exists across the cell boundary.

Heterogeneity of regional displacement was also measured in a focal plane near the cell apex (Fig. 2, *D–F*). Translation of segment groups was clearly visible in high-magnification insets (Fig. 2, *E* and *F*). Furthermore, filaments reaching over the nucleus were displaced into the focal plane after flow onset (Fig. 2 *D*), confirming that the distribution of IF movement was three-dimensional and not restricted to focal planes parallel to the coverslip. These data demonstrate that onset of shear stress induced significant displacement of IFs that was heterogeneously distributed in three dimensions.

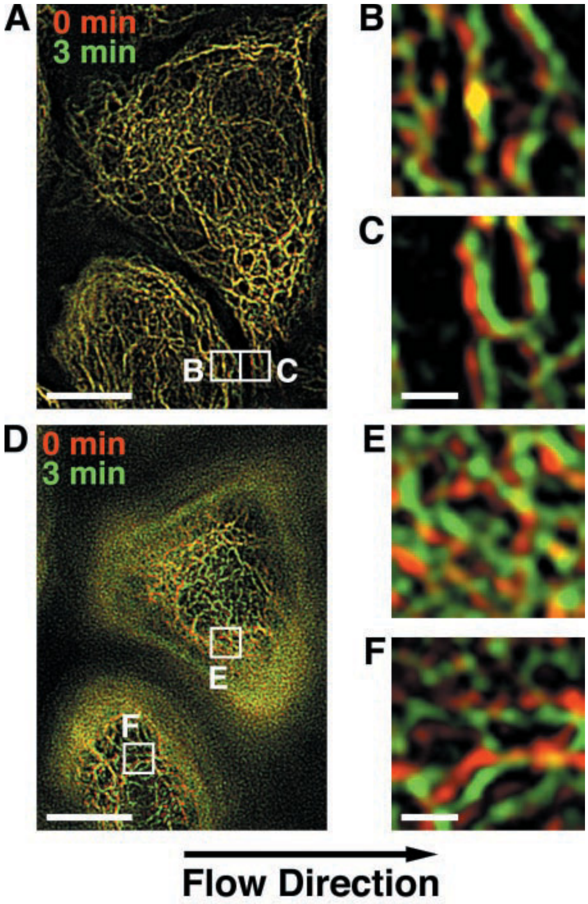

FIGURE 2 Merged color images of GFP-vimentin in optical sections just before (0 min, *red*) and 3 min after (*green*) flow onset (τ_w = 12 dyn cm^{-2}); yellow represents zero displacement during the interval. Flow direction in all images was left to right. (*A*) IF displacement in an optical section 1.0 μm above the coverslip. Scale bar, 10 μm. (*B*) Heterogeneity in IF motion in a higher magnification inset from *A*; IF bend and flex (*lower left*) or translate (*right*). (*C*) Coordinated translation of a group of IFs in an inset adjacent to *B*. Note that translation magnitude and direction is similar to that at the edge of the adjacent cell shown in *B*, suggesting a mechanical link between cells. Scale bar, 2 μm. (*D*) Optical section from the same cells but located 5 μm above the coverslip. Note in particular the appearance of green IFs overlying the nucleus, representing IFs that were displaced into the focal plane after flow onset. Scale bar, 10 μm. (*E–F*) Higher magnification insets from *D* showing significant IF displacement in these apical regions. Scale bar, 2 μm.

Spatial distribution of flow-induced IF movement

A displacement index, DI(t_i, t_j), was computed as a measure of the degree of filament movement during a time interval. If DI = 0, then the fluorescence intensity distribution functions overlap completely, indicating that no movement occurred during the interval. Increasing values of DI correspond to increased IF displacement during the interval. To map the spatial distribution of movement, fluorescence images were divided into 3-D subimages (Fig. 3) as described in Materials and Methods.

The spatial distribution of DI values in subimages was compared with merged color images that demonstrated IF movement (Fig. 4, *A* and *B*). Typically, small-magnitude constitutive motion of IFs was measured in the absence of shear stress (Fig. 4, *A*, *C*, *E*, and *G*). During the flow-onset interval, increased IF displacement was measured in cytoplasmic regions downstream and laterally from the nucleus (Fig. 4, *B*, *D*, *F*, and *H*). In contrast, no change in IF motion occurred in regions located directly below the nucleus (center of cell in Fig. 4 *D*). Strikingly, a consistent pattern of increased IF displacement with height in the cell emerged during the flow-onset interval.

Further comparison of the spatial distributions of DI during no-flow and flow-onset intervals revealed patterns in

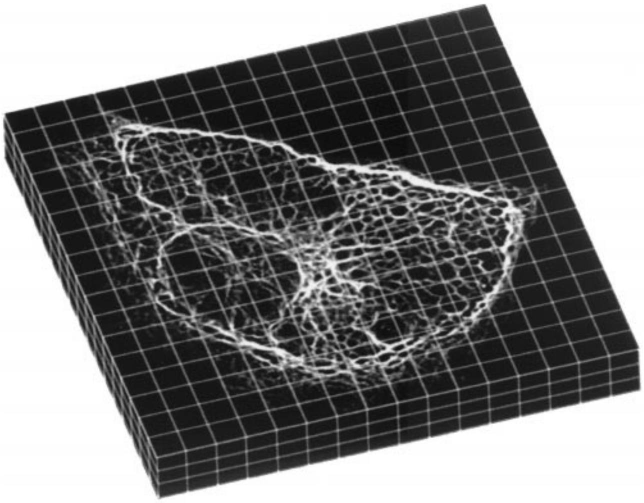

FIGURE 3 Example spatial grid demonstrating subdivision of GFP-vimentin fluorescence into 3-D subregions with size 3.4 μm × 3.4 μm × 1.7 μm.

flow-induced IF motion. In the cell studied in Fig. 5, onset of shear stress induced increased IF motion in most cytoplasmic regions (Fig. 5, *D*, *F*, and *H*) compared with the constitutive motion measured without flow (Fig. 5, *C*, *E*, and *G*). As in Fig. 4, flow-induced displacement increased with height in the cell. This is demonstrated in an *xz*-plane projection of a row of regions along the flow axis through the center of the cell (Fig. 5, *I–L*). Larger increases in DI were induced by flow near the apical surface than in other cytoplasmic regions, and increased IF motion was measured both on the upstream slope and directly above the nucleus. Flow-induced IF displacement was not constant at each height, indicating that IF deformation was spatially heterogeneous and not a simple shear deformation. Thus, shear stress applied to the lumenal surface may be transmitted through the cell in a manner that depends on cytoskeletal network morphology.

Patterns in the spatial distribution of IF displacement during flow onset were also measured in four adjacent cells within the same monolayer (Fig. 6, cells *a–d*). Near the coverslip in cell *b* (Fig. 6 *A*), increased displacement occurred in the downstream regions. In the adjacent cell downstream (Fig. 6, cell *c*), a similar pattern of increased DI was measured in regions along the trailing edge of the cell both near the coverslip (Fig. 6 *A*) and at a higher *z* position (Fig. 6 *B*). Near the apical surfaces, the largest displacements were measured above the nucleus and near the upstream edge of cell *b* (Fig. 6 *C*), whereas most flow-induced movement was located lateral to the nucleus in cell *c* (Fig. 6 *C*). In all four cells, flow-induced IF displacement clearly increased with height in the cell. IFs above the nucleus exhibited the largest deformations during the flow-onset interval (Fig. 6 *C*). These spatial maps of DI demonstrate

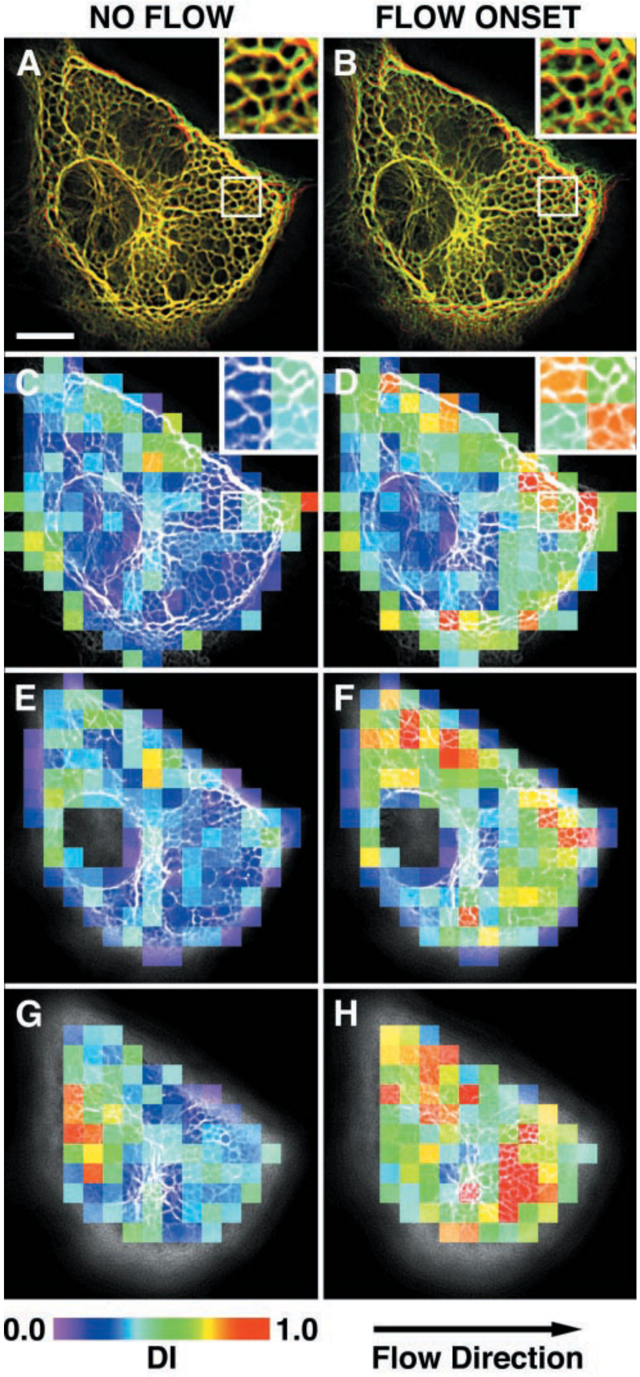

FIGURE 4 Spatial map of GFP-vimentin IF displacement during no-flow and flow-onset intervals. (*A* and *B*) Merged color images showing IF position near the coverslip ($z = 0.0–1.7$ μm) at the beginning (*red*) and end (*green*) of consecutive 3-min intervals with no flow (*A*) or immediately after flow onset (*B*) . (*Insets*) Regions of flow-induced IF displacement that exceeded constitutive displacement. (*C–H*) Color maps of DI that measure the magnitude of IF displacement near the coverslip ($z = 0.0–1.7$ μm; *C* and *D*), in mid-height regions ($z = 1.7–3.4$ μm; *E* and *F*), and near the lumenal surface ($z = 3.4–5.1$ μm; *G* and *H*). (*Insets*) Regions of color change indicating flow-induced alterations in DI. Flow direction is left to right. Subimage size, 3.4 μm × 3.4 μm × 1.7 μm. See text for discussion of spatial patterns of displacement.

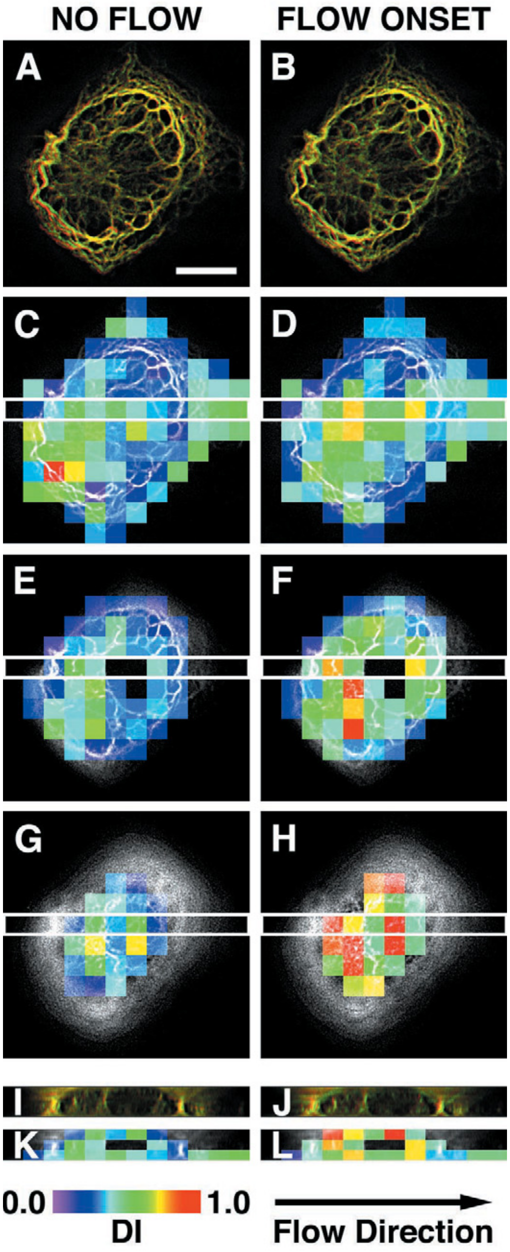

FIGURE 5 Spatial map of flow-induced IF displacement as a function of location in the cell. (*A* and *B*) Merged color images showing IF position near the coverslip ($z = 0.0–1.7\ \mu$m) at the beginning (*red*) and end (*green*) of consecutive 3-min intervals with no flow (*A*) or immediately after flow onset (*B*). (*C–H*) Color maps of DI showing distributions in *xy* projections near the coverslip ($z = 0.0–1.7\ \mu$m; *C* and *D*), in mid-height regions ($z = 1.7–3.4\ \mu$m; *E* and *F*), and near the lumenal surface ($z = 3.4–5.1\ \mu$m; *G* and *H*). (*I–J*) Merged color images of *xz* projections showing IF positions in the row of regions outlined in *C–H*. Merged color images show fluorescence distribution at the beginning (*red*) and end (*green*) of consecutive 3-min intervals with no flow (*I*) and immediately after flow onset (*J*). (*K–L*) DI color maps of *xz* projections illustrating variations in IF displacement with height but without preferential distribution of flow-induced displacement along the flow direction. Flow direction is left to right. Subimage size, 3.4 μm × 3.4 μm × 1.7 μm.

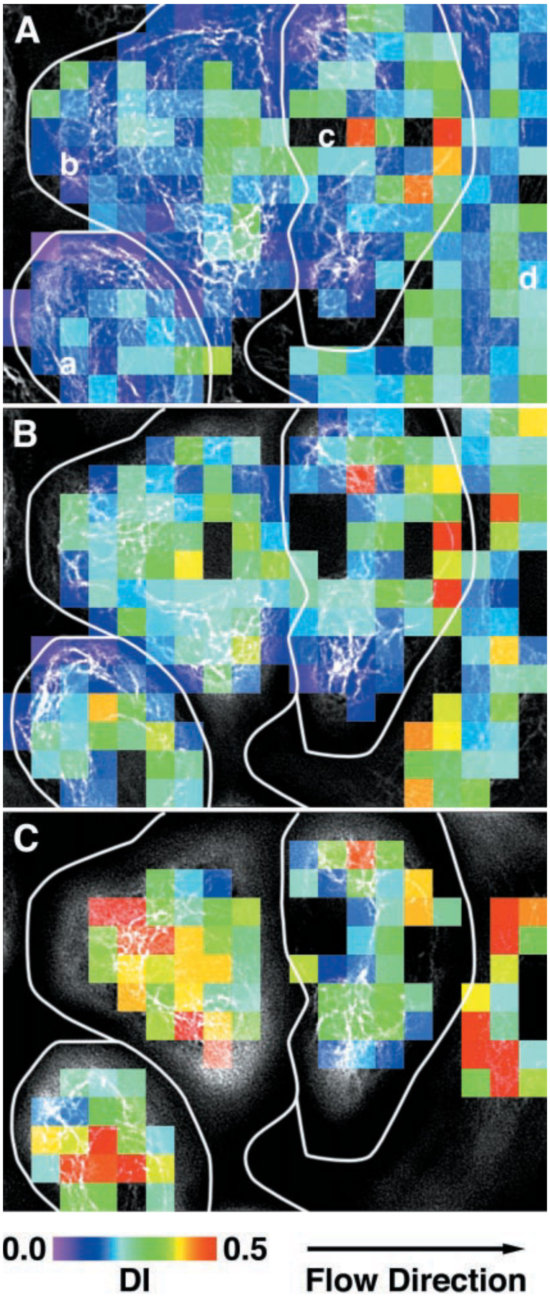

FIGURE 6 Spatial distribution of DI in a cell line with stable expression of GFP-vimentin during a 3-min flow-onset interval. Outlines of four neighboring cells (*a–d*) are illustrated. DI values in subimages are shown near the coverslip ($z = 0.0–1.7\ \mu$m; *A*), in mid-height regions ($z = 1.7–3.4\ \mu$m; *B*), and near the lumenal surface ($z = 3.4–5.1\ \mu$m; *C*). Flow direction is left to right. Subregion size, 3.4 μm × 3.4 μm × 1.7 μm. See text for discussion of spatial patterns of displacement.

quantitatively the spatial patterns of IF displacement among adjacent cells in response to flow onset.

A statistical comparison among spatial areas within ECs was performed to evaluate patterns of IF displacement. Subimages were grouped into six areas defined relative to flow direction and nuclear position: upstream, downstream, left, right, below, and above. Expected values and 95% confidence intervals for DI were computed for each spatial area (Table 1), and all-pairwise comparisons between groups during the flow-onset interval were performed (Newman-Keuls procedure). In a single cell during the flow-onset interval, DI did not vary significantly among lateral regions of the cell, including upstream and downstream from the nucleus. However, DI in the area below the nucleus was significantly smaller than in the other five areas in the cell, as DI increased during the flow-onset interval in most cell regions relative to that below the nucleus. These significant differences ($p < 0.05$) among DI values were mapped schematically (Fig. 7). Comparisons within a single cell (Fig. 7 *A*) confirmed quantitatively the trends in flow-induced differences observed in spatial maps of DI values (see Fig. 4).

Statistical comparisons were performed in a similar manner for DI values from nine cells (Table 1). Although spatial maps of DI varied from cell to cell, pooled data exhibited interesting trends in the pattern of intracellular IF displacement (Fig. 7 *B*). DI values in the area above the nucleus were significantly larger than those below the nucleus. Larger IF displacement may be expected near the lumenal surface where shear stress forces act directly. Similarly, IF displacement below the nucleus may be smaller than in other areas due to relative stability in this area. DI in areas above and below the nucleus was larger and smaller, respectively, than in areas either upstream or left, indicating spatial gradients in the degree of IF displacement. Finally, the area downstream from the nucleus was displaced more than the upstream, left, or right areas in the cell. This implies that IF displacement may depend on connections among filaments in the network in addition to a direct response to flow forces on the upstream surface of the cell. Taken together, these results indicate that, on average, flow-induced IF displacement increases with height in the cell, and variability of spatial gradients of displacement may be related to structural differences among cells.

TABLE 1 Expected values and 95% confidence intervals for DI during the flow-onset interval in areas of cells defined relative to nuclear position and flow direction as illustrated in Fig. 7

	One cell		Nine cells	
	DI	95% CI	DI	95% CI
Upstream	0.36	(0.28, 0.46)	0.32	(0.29, 0.35)
Downstream	0.44	(0.40, 0.49)	0.38	(0.35, 0.42)
Left	0.52	(0.45, 0.61)	0.29	(0.26, 0.32)
Right	0.35	(0.28, 0.43)	0.26	(0.24, 0.29)
Below	0.19	(0.16, 0.23)	0.22	(0.20, 0.25)
Above	0.53	(0.46, 0.61)	0.44	(0.39, 0.49)

Data were from a single cell or pooled from nine cells from six separate experiments. Significant differences in pairwise comparisons are mapped schematically in Fig. 7.

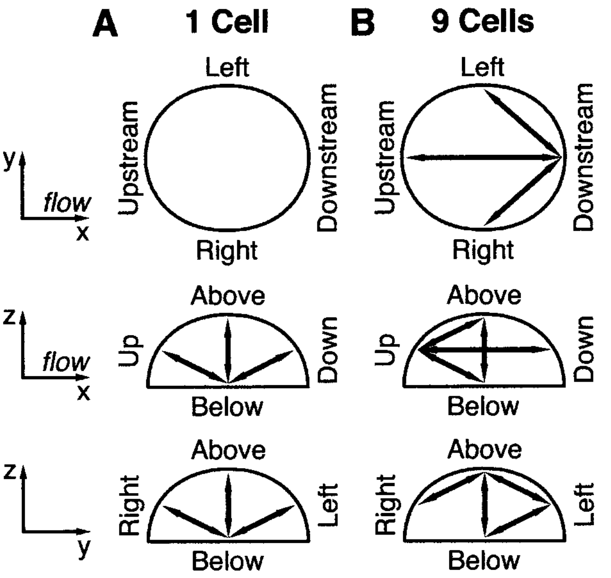

FIGURE 7 Schematic diagram of spatial differences in DI during 3-min flow-onset interval mapped relative to flow direction and nuclear position in a single cell within the monolayer (*A*) and computed from pooled data from nine cells in six experiments (*B*). Diagrams show schematic representations of cell projections onto *xy*, *xz*, and *yz* planes, as indicated. Flow direction was parallel to the *x* axis. DI distributions in subregions located upstream, downstream, left, right, below, and above the nucleus were compared. As described in Materials and Methods, all-pairwise comparisons among DI values (see Table 1) in each spatial area were performed (Newman-Keuls procedure). Bold arrows show pairs of areas that were significantly different from each other ($p < 0.05$). Note that the results in *A* were computed for the cell shown in Fig. 4.

Temporal distribution of flow-induced IF movement

Comparison of DI values before, during, and after flow onset in subregions of cells confirmed that significant displacement occurred with the onset of flow (Fig. 8) but not during the succeeding continued-flow intervals. To characterize IF displacement in a cell with respect to time, DI values in each subimage were plotted as a function of time interval and height region (Fig. 8 *A*), and 95% confidence intervals for each height and time interval were computed (Fig. 8 *B*). During consecutive 3-min intervals with no flow, small variations in DI occurred; however, the confidence intervals remained constant, indicating a steady-state constitutive motion of IFs. Both the magnitude of displacement and the variability in DI among spatial regions were increased with height in the cell during the flow-onset interval. DI was decreased during the succeeding flow interval and reached a new steady state in the continued presence of shear stress.

To describe more precisely the spatial distribution of flow-induced changes, pairwise comparisons were performed between consecutive no-flow and flow-onset intervals within spatial areas defined relative to flow direction

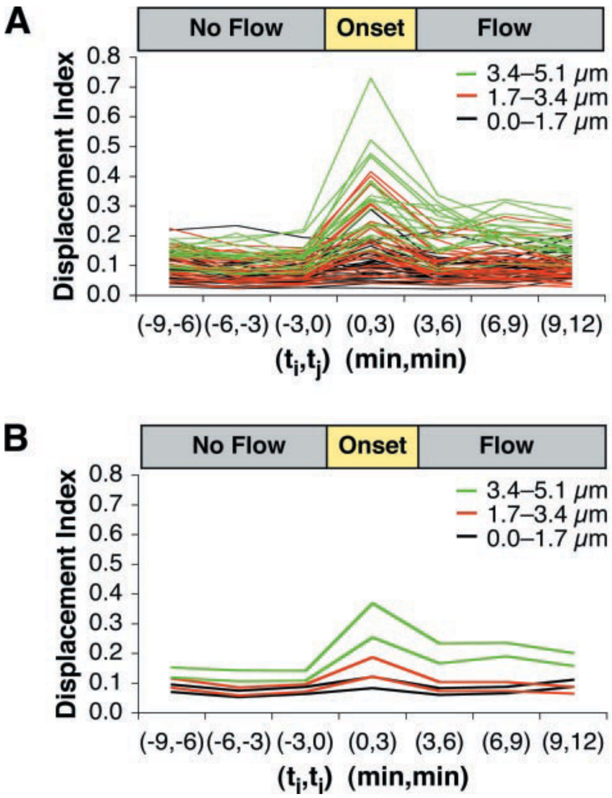

FIGURE 8 DI distribution in a single cell grouped by height for consecutive 3-min intervals with no flow, immediately after flow onset, and in the presence of continued flow. (*A*) Increase in magnitude and variability of DI computed from individual subimages during flow onset, followed by less variation with continued flow. The degree and variability of displacement during flow-onset interval increased with height in the cell. (*B*) The 95% confidence intervals computed from DI values in *A* and grouped by height in the cell. For all height groups, DI increased significantly ($p < 0.05$) during the flow-onset interval compared with the previous no-flow interval. Furthermore, DI during the flow-onset interval was significantly different among height groups ($p < 0.05$).

and nuclear position. As in Fig. 7, six areas were examined: upstream, downstream, left, right, below, and above the nucleus. The percent change in DI from no-flow to flow-onset interval was computed for areas of nine cells individually and for pooled data (Table 2). Flow onset induced increased displacement in nearly all spatial regions of cells; decreases were rarely observed. Although flow-induced changes in DI were variable among regions and from cell to cell, several trends were noted. Within individual cells, DI below the nucleus increased significantly with flow onset in only one of nine cells, and no significant differences were measured in upstream regions of nine cells ($p < 0.05$, Newman-Keuls procedure). However, in an area above the nucleus, DI increased significantly in five of nine cells. Flow onset tended to act primarily in areas of the cell near the lumenal surface. Although data from individual cells was variable, comparisons between time intervals for pooled data from nine cells demonstrated a significant effect of flow onset in all areas except below the nucleus. Thus, during the flow-onset interval, IF displacement was increased significantly over constitutive motion except in regions located below the nucleus that may be mechanically stabilized relative to areas near the lumenal surface.

TABLE 2 Percent change in DI from no-flow to flow-onset interval in areas of cells defined relative to nuclear position and flow direction as in Fig. 7

	Upstream	Downstream	Left	Right	Below	Above
Cell 1	+54	+160*	+74	N/A	+17	+203*
Cell 2	+36	+36	+34	+75*	+15	+96*
Cell 3	N/A	+136*	+109*	+71	+75*	+143*
Cell 4	+58	N/A	+34	+54	+23	+73
Cell 5	+76	+73	+108	+39	+27	+91*
Cell 6	−6	+82*	+63*	+63*	−9	0
Cell 7	+48	+18	+81	−8	−3	+22
Cell 8	+26	+24	+18	+14	+3	+66*
Cell 9	+30	+35	+37	+31	+18	+14
Pooled	+38*	+73*	+54*	+45*	+14	+64*

Data were not available for regions near the edge of an image in cells 1, 3, and 4. Values in the last row were computed from pooled data from areas of nine cells from six separate experiments. Pairwise comparisons were performed between no-flow and flow-onset intervals within each region using the Newman-Keuls procedure as described in the text.
*$p < 0.05$.

DISCUSSION

Shear stress acting on the lumenal surface of endothelial cells contributes to the physiological regulation of the vessel wall through multiple interactions among intracellular signaling networks (reviewed in Davies, 1995). These cellular mechanotransduction mechanisms may be potentiated in part by structural adaptation of vessel wall cells to local variations in arterial hemodynamics. Adaptation of cellular shape and reorganization of cytoskeletal networks has been measured after hours of unidirectional laminar flow in vitro (Dewey et al., 1981; Levesque and Nerem, 1985; Malek and Izumo, 1996; Galbraith et al., 1998). As a result, previous automated methods to measure cellular adaptation have focused on characterizing the distribution of cellular orientation using Fourier (Kohler et al., 1994; Palmer and Bizios, 1997) or texture-based (Karlon et al., 1999) methods. However, rapid deformation of cytoskeletal filaments has been demonstrated within minutes after introducing an altered hemodynamic profile (Helmke et al., 2000). On this shorter time scale, morphometric parameters describing the cellular length scale are not expected to change. Instead, characterization of adaptation at a subcellular length scale is required. Thus, a quantitative method has been developed to analyze IF displacement magnitude as a 4-D function of space and time during the first few minutes after onset of shear stress.

A spatiotemporal analysis of IF displacement using DI has several advantages over previous methods. Because fluorescence intensity distributions are compared in three dimensions, detection of IF movement along the optical axis is possible. A 3-D measurement often revealed IF displacement that was not visible in 2-D projection images. Because DI is insensitive to the absolute fluorescence intensity magnitude, a detailed quantitative comparison of the spatial distribution of IF movement can be performed without correction for minor fluctuation in image brightness. In addition to changes in average filament orientation, DI also includes IF translation in 3-D. As a result, filament displacement was measured in cases where filament or local network shape did not change. Finally, DI measures movement of IFs on a subcellular length scale, allowing measurement of an intracellular distribution of displacement that is not visible at a longer whole-cell length scale. Furthermore, the length scale can be chosen to include relevant morphological features of interest by adjusting the subimage size over which the DI is computed.

The DI defined here represents the first computational result to quantitatively compare 4-D fluorescence intensity functions acquired from living ECs. To gain the most information from the fluorescence data, however, high-resolution image sets with adequate signal-to-noise ratio must be obtained. Because the PMCC within the DI computation measures the degree of overlap of fluorescence intensity distribution functions, sensitivity to IF displacement depends to some extent on the width of fluorescence peaks corresponding to filament positions. Thus, low-resolution or low-contrast images would limit the ability to detect changes in IF position. Furthermore, systematic errors during data acquisition due to coverslip movement may result in false interpretation of the degree of IF movement. In the present study, the ability to detect IF displacement was maximized by image restoration (Hiraoka et al., 1990) and normalization for coverslip position using fluorescent microspheres.

Satcher and Dewey (1996) predicted a Young's modulus of order 10^5 dyn/cm^2 for ECs using an open-cell foam model. The F-actin cytoskeleton was represented as an interconnecting lattice of cubic unit cells that deformed at their edges. However, the corners of the unit cell, which represented filament cross-links, were considered to be rigid. The predicted Young's modulus may therefore represent an upper bound on the range for whole cells. The composite modulus is more likely determined by more complicated and heterogeneous intracellular structures that allow for filament interactions and flexible connections. Although the IF movement measured here was spatially heterogeneous, the absolute displacement magnitudes of individual IFs within the network (Helmke et al., 2000) were consistent with other measurements of mechanical properties in polymer gels (Janmey et al., 1991) and in intact cells (Schmid-Schönbein et al., 1981; Dong et al., 1988; Theret et al., 1988; Needham and Hochmuth, 1990; Haga et al., 1998). The median displacement of 35 randomly chosen IF positions after 3 min of exposure to shear stress of 12 dyn/cm^2 was $\sim$0.2 μm (Helmke et al., 2000). For a simple shear deformation of a cell with height 5 μm, this corresponds to a shear modulus of order 300 dyn/cm^2. In vitro measurements on gels of polymerized actin or vimentin predict shear moduli of 2830 dyn/cm^2 and 320 dyn/cm^2, respectively (Janmey et al., 1991). Interestingly, the elastic modulus of a copolymerized actin-vimentin mixture was $\sim$1/3 that of pure actin (Janmey et al., 1998), suggesting that interactions between different cytoskeleton networks play a significant role in determining mechanical properties. Using micropipet aspiration techniques, the effective Young's modulus has been estimated to be $\sim 10^3$ dyn/cm^2 for ECs (Theret et al., 1988) and platelets (Haga et al., 1998), and the Young's modulus for neutrophils lies in the range 200–400 dyn/cm^2 (Schmid-Schönbein et al., 1981; Dong et al., 1988). Thus, the magnitude of IF deformation measured here is consistent with experimentally measured cytoplasmic viscoelastic properties.

Spatial maps of DI (Figs. 4–6) represent the instantaneous strain magnitude distribution as a function of time. Whereas previous studies have measured average cytoskeletal strain using internalized microsphere markers (Simon and Schmid-Schönbein, 1990; Caille et al., 1998), 4-D GFP-vimentin fluorescence allows measurement of network strain distribution directly from IF positions. The computation of flow-induced cytoskeletal network strain has several important implications for understanding cellular biomechanics, as suggested by theoretical modeling of a shear stress influence on actin dynamics (Suciu et al., 1997). Prediction of fluid shear force distribution on the endothelial surface has been computed from topographical maps measured by atomic force microscopy (Barbee et al., 1995). The maximum shear stress acts on the plasma membrane at peaks in topography located over the nucleus. Pooled DI computations for the nine cells studied here demonstrate that IF displacement during flow onset was significantly larger in the area above the nucleus than in most other areas of the cytoplasm, suggesting a significant force redistribution to that region. However, the interpretation of force transmission to those IFs is complicated by variability in measurements among cells. For example, flow onset also induced increased IF displacement in other lateral regions of a cell so that motion above the nucleus, although larger in magnitude, was not significantly different. Nevertheless, the pattern of increased IF movement above the nucleus was consistent in most cells.

During the flow-onset interval, a pattern of increased IF displacement was consistently measured (Fig. 8), even though significant heterogeneity was observed in the spatial pattern in individual cells. Furthermore, spatial analysis of changes in the DI during flow onset compared with no-flow intervals (Table 2) demonstrated that regional IF displacement was rarely decreased by onset of shear stress. The increased IF displacements measured here suggest that hemodynamic forces acting on the lumenal plasma membrane altered the tension distribution in the IF network. Force may be transmitted to IF through apical plaques (Kano et al., 1996), focal adhesion-like structures that serve as insertion points for actin stress fibers. Vimentin interacts directly with both actin stress fibers and phosphoinositide lipids in vitro (Shah et al., 1998), and indirect interactions between IF and stress fibers is possible through cross-linking molecules such as plectin (Goldman et al., 1986; Flitney et al., 1996; Svitkina et al., 1996). Thus, we propose that the magnitude and/or local gradients of shear stress acting at the cell surface (Barbee et al., 1995) are transmitted heterogeneously in a manner that depends on cytoskeletal network morphology and physical interactions among structural components. This redistribution of cytoplasmic force away from the apical plasma membrane may contribute to alterations in structural dynamics and signaling responses at other locations in the cell (Davies et al., 1993, 1994; Berk et al., 1995), including focal adhesion sites (Ingber, 1991; Ishida et al., 1996; Schmidt et al., 1998; Wernick et al., 1998) and cell-cell junctions (DePaola et al., 1999; Noria et al., 1999).

Another possible mechanism for flow-induced IF motion involves biochemical regulation of IF dynamics. Mechanotransduction results in activation of multiple signaling networks (Davies and Tripathi, 1993; Chen et al., 1999; Yan et al., 1999) that may affect IF dynamics. For example, vimentin polymerization is affected to some extent by phosphorylation state (Eriksson et al., 1992), suggesting that activation of kinases and/or phosphatases by mechanical stimuli may also participate in regulating IF structure. The importance of this mechanism and its ability to achieve the observed spatial heterogeneity in IF displacement remains unclear, however.

The DI provides a quantitative description of the subcellular distribution of IF displacement magnitude. It is sensitive to the degree of 3-D IF motion during a specified time interval. Further development of this method is in progress that will take advantage of the 3-D cross-correlation computation among discrete time intervals to derive both the magnitude and direction of IF displacement. This will facilitate prediction of a direct spatial relationship between hemodynamic force and cytoskeletal displacement.

In summary, the measurement of IF positions in living ECs during onset of shear stress reveals new details about cytoskeletal displacement at a subcellular length scale in response to a physiological mechanical stimulus. Because cytoskeletal movement is directly related to intracellular force transmission, this analysis provides new insights into mechanisms of endothelial responses to an altered hemodynamic environment.

We thank J. Murray for helpful discussion in the development of PMCC computations and D. Hammer for critical reading of the manuscript.

This work was supported by National Institutes of Health NRSA grant HL10058 (B.P.H.), University of Pennsylvania SEAS undergraduate research grant (D.B.T.), National Institutes of Health MERIT grant GM36806 (R.D.G.), and National Institutes of Health P32 grant HL62250 and MERIT grant HL36049 (P.F.D.).

REFERENCES

Ballestrem, C., B. Wehrle-Haller, and B. A. Imhof. 1998. Actin dynamics in living mammalian cells. *J. Cell Sci.* 111:1649–1658.

Barbee, K. A., T. Mundel, R. Lal, and P. F. Davies. 1995. Subcellular distribution of shear stress at the surface of flow-aligned and nonaligned endothelial monolayers. *Am. J. Physiol.* 268:H1765–H1772.

Batchelor, G. K. 1967. An Introduction to Fluid Mechanics. Cambridge University Press, Cambridge, UK.

Berk, B. C., M. A. Corson, T. E. Peterson, and H. Tseng. 1995. Protein kinases as mediators of fluid shear stress stimulated signal transduction in endothelial cells: a hypothesis for calcium-dependent and calcium-independent events activated by flow. *J. Biomech.* 28:1439–1450.

Blose, S. H., and D. I. Meltzer. 1981. Visualization of the 10-nm filament vimentin rings in vascular endothelial cells in situ: close resemblance to vimentin cytoskeletons found in monolayers in vitro. *Exp. Cell Res.* 135:299–309.

Burridge, K., and M. Chrzanowska-Wodnicka. 1996. Focal adhesions, contractility, and signaling. *Annu. Rev. Cell Dev. Biol.* 12:463–518.

Caille, N., Y. Tardy, and J. J. Meister. 1998. Assessment of strain field in endothelial cells subjected to uniaxial deformation of their substrate. *Ann. Biomed. Eng.* 26:409–416.

Carminati, J. L., and T. Stearns. 1997. Microtubules orient the mitotic spindle in yeast through dynein-dependent interactions with the cell cortex. *J. Cell Biol.* 138:629–641.

Chen, K. D., Y. S. Li, M. Kim, S. Li, S. Yuan, S. Chien, and J. Y. Shyy. 1999. Mechanotransduction in response to shear stress: roles of receptor tyrosine kinases, integrins, and Shc. *J. Biol. Chem.* 274:18393–18400.

Chien, S., S. Li, and J. Y. J. Shyy. 1998. Effects of mechanical forces on signal transduction and gene expression in endothelial cells. *Hypertension.* 31:162–169.

Choquet, D., D. P. Felsenfeld, and M. P. Sheetz. 1997. Extracellular matrix rigidity causes strengthening of integrin-cytoskeleton linkages. *Cell.* 88:39–48.

Davies, P. F. 1995. Flow-mediated endothelial mechanotransduction. *Physiol. Rev.* 75:519–560.

Davies, P. F., A. Robotewskyj, and M. L. Griem. 1993. Endothelial cell adhesion in real time: measurements in vitro by tandem scanning confocal image analysis. *J. Clin. Invest.* 91:2690–2652.

Davies, P. F., A. Robotewskyj, and M. L. Griem. 1994. Quantitative studies of endothelial cell adhesion: directional remodeling of focal adhesion sites in response to flow forces. *J. Clin. Invest.* 93:2031–2038.

Davies, P. F., and S. C. Tripathi. 1993. Mechanical stress mechanisms and the cell: an endothelial paradigm. *Circ. Res.* 72:239–245.

DePaola, N., P. F. Davies, W. F. Pritchard, Jr., L. Florez, N. Harbeck, and D. C. Polacek. 1999. Spatial and temporal regulation of gap junction connexin43 in vascular endothelial cells exposed to controlled disturbed flows in vitro. *Proc. Natl. Acad. Sci. U.S.A.* 96:3154–3159.

Dewey, C. F., Jr., S. R. Bussolari, M. A. Gimbrone, Jr., and P. F. Davies. 1981. The dynamic response of vascular endothelial cells to fluid shear stress. *J. Biomech. Eng.* 103:177–185.

Dong, C., R. Skalak, K.-L. P. Sung, G. W. Schmid-Schönbein, and S. Chien. 1988. Passive deformation analysis of human leukocytes. *J. Biomech. Eng.* 110:27–36.

Doyle, T., and D. Botstein. 1996. Movement of yeast cortical actin cytoskeleton visualized in vivo. *Proc. Natl. Acad. Sci. U.S.A.* 93:3886–3891.

Eriksson, J. E., P. Opal, and R. D. Goldman. 1992. Intermediate filament dynamics. *Curr. Opin. Cell Biol.* 4:99–104.

Flitney, F. W., R. D. Goldman, O. Skalli, K. O. Mercurius, and P. F. Davies. 1996. Dynamic properties of intermediate filaments in cultured endothelial cells: the effects of controlled fluid shear stress. *In* The

Biology of Nitric Oxide. S. Moncada, J. Stamler, S. Gross, and E. A. Higgs, editors. Portland Press, London. 251.

Galbraith, C. G., R. Skalak, and S. Chien. 1998. Shear stress induces spatial reorganization of the endothelial cell cytoskeleton. *Cell Motil. Cytoskel.* 40:317–330.

Goldman, R. D., A. E. Goldman, K. J. Green, J. C. R. Jones, S. M. Jones, and H.-Y. Yang. 1986. Intermediate filament networks: organization and possible functions of a diverse group of cytoskeletal elements. *J. Cell Sci. (Suppl.)* 5:69–97.

Haga, J. H., A. J. Beaudoin, J. G. White, and J. Strony. 1998. Quantification of the passive mechanical properties of the resting platelet. *Ann. Biomed. Eng.* 26:268–277.

Heidemann, S. R., S. Kaech, R. E. Buxbaum, and A. Matus. 1999. Direct observation of the mechanical behaviors of the cytoskeleton in living fibroblasts. *J. Cell Biol.* 145:109–122.

Helmke, B. P., R. D. Goldman, and P. F. Davies. 2000. Rapid displacement of vimentin intermediate filaments in living endothelial cells exposed to flow. *Circ. Res.* 86:745–752.

Hiraoka, Y., J. W. Sedat, and D. A. Agard. 1990. Determination of three-dimensional properties of a light microscope system: partial confocal behavior in epifluorescence microscopy. *Biophys. J.* 57:325–333.

Ho, C.-L., J. L. Martys, A. Mikhailov, G. G. Gundersen, and R. K. H. Liem. 1998. Novel features of intermediate filament dynamics revealed by green fluorescent protein chimeras. *J. Cell Sci.* 111:1767–1778.

Ingber, D. 1991. Integrins as mechanochemical transducers. *Curr. Opin. Cell Biol.* 3:841–848.

Ishida, T., T. E. Peterson, N. L. Kovach, and B. C. Berk. 1996. MAP kinase activation by flow in endothelial cells: role of β_1 integrins and tyrosine kinases. *Circ. Res.* 79:310–316.

Janmey, P. A., U. Euteneuer, P. Traub, and M. Schliwa. 1991. Viscoelastic properties of vimentin compared with other filamentous biopolymer networks. *J. Cell Biol.* 113:155–160.

Janmey, P. A., J. V. Shah, K.-P. Janssen, and M. Schliwa. 1998. Viscoelasticity of intermediate filament networks. *Subcell. Biochem.* 31:381–397.

Kam, Z., M. O. Jones, H. Chen, D. A. Agard, and J. W. Sedat. 1993. Design and construction of an optimal illumination system for quantitative wide-field multi-dimensional microscopy. *Bioimaging.* 1:71–81.

Kano, Y., K. Katoh, M. Masuda, and K. Fujiwara. 1996. Macromolecular composition of stress fiber-plasma membrane attachments sites in endothelial cells in situ. *Circ. Res.* 79:1000–1006.

Karlon, W. J., P.-P. Hsu, S. Li, S. Chien, A. D. McCulloch, and J. H. Omens. 1999. Measurement of orientation and distribution of cellular alignment and cytoskeletal organization. *Ann. Biomed. Eng.* 27: 712–720.

Kohler, M., M. Aufderheide, and D. Ramm. 1994. Method for the description of differences in the filamentous structure of the cytoskeleton in cultured cells. *Toxicol. Lett.* 72:33–42.

Levesque, M. J., and R. M. Nerem. 1985. The elongation and orientation of cultured endothelial cells in response to shear stress. *J. Biomech. Eng.* 107:341–347.

Malek, A. M., and S. Izumo. 1996. Mechanism of endothelial cell shape change and cytoskeletal remodeling in response to fluid shear stress. *J. Cell Sci.* 109:713–726.

Needham, D., and R. M. Hochmuth. 1990. Rapid flow of passive neutrophils into a 4 μm pipet and measurement of cytoplasmic viscosity. *J. Biomech. Eng.* 112:269–276.

Nerem, R. M., M. J. Levesque, and J. F. Cornhill. 1981. Vascular endothelial morphology as an indicator of the pattern of blood flow. *J. Biomech. Eng.* 103:172–176.

Noria, S., D. B. Cowan, A. I. Gotlieb, and B. L. Langille. 1999. Transient and steady-state effects of shear stress on endothelial cell adherens junctions. *Circ. Res.* 85:504–514.

Palmer, B. M., and R. Bizios. 1997. Quantitative characterization of vascular endothelial cell morphology and orientation using Fourier transform analysis. *J. Biomech. Eng.* 119:159–165.

Petroll, W. M., H. D. Cavanaugh, P. Barry, P. Andrews, and J. V. Jester. 1993. Quantitative analysis of stress fiber orientation during corneal wound contraction. *J. Cell Sci.* 104:353–363.

Resnick, N., H. Yahav, L. M. Khachigian, T. Collins, K. R. Anderson, C. F. Dewey, Jr., and M. A. Gimbrone, Jr. 1997. Endothelial gene regulation by laminar shear stress. *Adv. Exp. Med. Biol.* 430:155–164.

Satcher, R. L., Jr., and C. F. Dewey, Jr. 1996. Theoretical estimates of mechanical properties of the endothelial cell cytoskeleton. *Biophys. J.* 71:109–118.

Schmid-Schönbein, G. W., K.-L. P. Sung, H. Tözeren, R. Skalak, and S. Chien. 1981. Passive mechanical properties of human leukocytes. *Biophys. J.* 36:243–256.

Schmidt, C., H. Pommerenke, F. Dürr, B. Nebe, and J. Rychly. 1998. Mechanical stressing of integrin receptors induces enhanced tyrosine phosphorylation of cytoskeletally anchored proteins. *J. Biol. Chem.* 273:5081–5085.

Shah, J. V., L. Z. Wang, P. Traub, and P. A. Janmey. 1998. Interaction of vimentin with actin and phospholipids. *Biol. Bull.* 194:402–405.

Simon, S. I., and G. W. Schmid-Schönbein. 1990. Kinematics of cytoplasmic deformation in neutrophils during active motion. *J. Biomech. Eng.* 112:303–310.

Suciu, A., G. Civelekoglu, Y. Tardy, and J. J. Meister. 1997. Model for the alignment of actin filaments in endothelial cells subjected to fluid shear stress. *Bull. Math. Biol.* 59:1029–1046.

Svitkina, T. M., A. B. Verkhovsky, and G. G. Borisy. 1996. Plectin sidearms mediate interaction of intermediate filaments with microtubules and other components of the cytoskeleton. *J. Cell Biol.* 135: 991–1007.

Theret, D. P., M. J. Levesque, M. Sato, R. M. Nerem, and L. T. Wheeler. 1988. The application of a homogeneous half-space model in the analysis of endothelial cell micropipette measurements. *J. Biomech. Eng.* 110:190–199.

Wernick, M. N., M. L. Griem, A. Robotewskyj, and P. F. Davies. 1998. Image analysis of the dynamic changes of adhesion sites in endothelial cells subjected to directional flow in vitro. *J. Vasc. Invest.* 4:15–23.

Westphal, M., A. Jungbluth, M. Heidecker, B. Muhlbauer, C. Heizer, J. M. Schwartz, G. Marriott, and G. Gerisch. 1997. Microfilament dynamics during cell movement and chemotaxis monitored using a GFP-actin fusion protein. *Curr. Biol.* 7:176–183.

Yan, C., M. Takahashi, M. Okuda, J. D. Lee, and B. C. Berk. 1999. Fluid shear stress stimulates big mitogen-activated protein kinase 1 (BMK1) activity in endothelial cells: dependence on tyrosine kinases and intracellular calcium. *J. Biol. Chem.* 274:143–150.

Yoon, M., R. D. Moir, V. Prahlad, and R. D. Goldman. 1998. Motile properties of vimentin intermediate filament networks in living cells. *J. Cell Biol.* 143:147–157.